ORIGINAL PAPER

Parallel evolution of semicircular canal form and sensitivity in subterranean mammals

Jana Goyens[1] · Simon Baeckens[1,2] · Ewan St. John Smith[3] · Jasmine Pozzi[1] · Matthew J. Mason[4]

Abstract

The vertebrate vestibular system is crucial for balance and navigation, and the evolution of its form and function in relation to species' lifestyle and mode of locomotion has been the focus of considerable recent study. Most research, however, has concentrated on aboveground mammals, with much less published on subterranean fauna. Here, we explored variation in anatomy and sensitivity of the semicircular canals among 91 mammal species, including both subterranean and non-subterranean representatives. Quantitative phylogenetically informed analyses showed significant widening of the canals relative to radius of curvature in subterranean species. A relative canal width above 0.166 indicates with 95% certainty that a species is subterranean. Fluid–structure interaction modelling predicted that canal widening leads to a substantial increase in canal sensitivity; a reasonably good estimation of the absolute sensitivity is possible based on the absolute internal canal width alone. In addition, phylogenetic comparative modelling and functional landscape exploration revealed repeated independent evolution of increased relative canal width and anterior canal sensitivity associated with the transition to a subterranean lifestyle, providing evidence of parallel adaptation. Our results suggest that living in dark, subterranean tunnels requires good balance and/or navigation skills which may be facilitated by more sensitive semicircular canals.

Keywords Internal canal width · Functional landscape · Fluid–structure interaction model · Semicircular canal · Subarcuate fossa

Introduction

The vestibular system of the vertebrate inner ear facilitates orientation, gives rise to a sense of self-motion (Angelaki and Cullen 2008), is crucial for balance (Cherng et al. 2001; Fitzpatrick and Day 2004), and plays an important role in navigation through a sense of spatial awareness and by providing input for path integration (Mittelstaedt 1999;

✉ Jana Goyens
jana.goyens@uantwerpen.be

1   Laboratory of Functional Morphology, University of Antwerp, Antwerp, Belgium

2   Evolution and Optics of Nanostructures Lab, Department of Biology, Ghent University, Ghent, Belgium

3   Department of Pharmacology, University of Cambridge, Cambridge, UK

4   Department of Physiology, Development and Neuroscience, University of Cambridge, Cambridge, UK

Stackman and Herbert 2002; Yoder and Taube 2014). The vestibular system does so by sensing head accelerations: its three semicircular canals (SCCs; Fig. 1) perceive head rotations, while its otolith organs are stimulated by head translations (Angelaki and Cullen 2008; Yoder and Taube 2014). The vestibular system comprises tunnels within the petrosal bone (the bony labyrinth) which are filled with perilymphatic fluid. Using the terminology of Ekdale (2016), we refer to the tunnels within the bone as 'canals' and the membranous tubes within the canals, which contain endolymphatic fluid, as 'ducts'. Each of the slender canals widens at one end into a chamber, the ampulla, where the sensory organ is located. During head rotation, the endolymph fluid lags behind the movement of the head (Rabbitt et al. 2004; Angelaki and Cullen 2008). However, because the cupulae seal the semicircular canals like diaphragms (McLaren and Hillman 1979; Rabbitt et al. 2004, 2009), they push forward the body of endolymph that runs from one side of the ampulla, through the slender duct, common crus (in case of the anterior and posterior canal), and utricle toward the other side of the ampulla (Goyens and Aerts 2019; Jiang

Fig. 1 Bony labyrinths of a *H. glaber* (**A**) and *M. musculus* (**B**) specimen. Anatomical measurements are illustrated on **A**. D1 and D2, diameters of the annulus formed by the SCC in two perpendicular directions, shown for the horizontal SCC; d, internal canal width, shown for the anterior SCC; AC, anterior SCC; PC, posterior SCC; HC, horizontal SCC; V, vestibule; a, ampulla; c, common crus
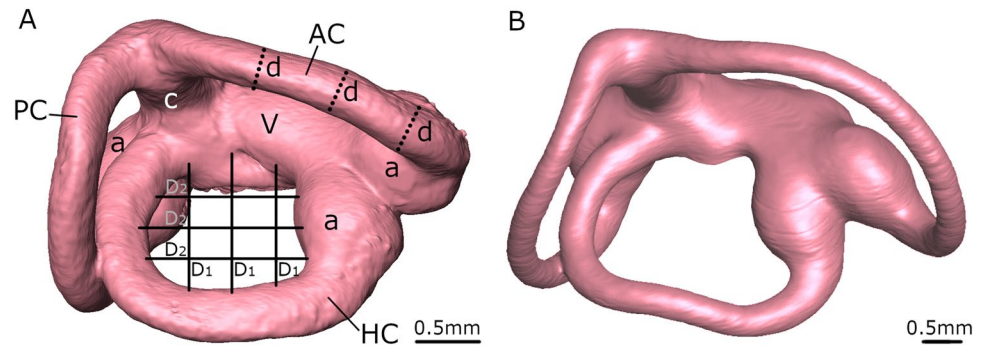
et al. 2022). The resulting pressure difference on the cupula deforms this flexible membrane, thereby deflecting the stereocilia on the associated hair cells, ultimately giving rise to an electrical signal (Rabbitt et al. 2004).

The sensitivity of the SCCs depends upon duct size and shape (e.g. Gray 1907; Spoor et al. 2007; Billet et al. 2012; Malinzak et al. 2012; Grohé et al. 2016; Pfaff et al. 2017). It has long been recognised that the overall size of an animal's SCCs relates to its locomotion behaviour (Gray 1907). This notion gained momentum from the influential investigation by Spoor et al. (2007) of a large dataset of over 200 mammalian species, which showed that fast, agile animals have larger SCCs (measured by the radius of curvature) relative to their body mass than more cautiously moving animals. A number of follow-up studies found additional correlations between the shape of the SCCs and the locomotion style or habitat of a particular species. For example, arboreal marsupials have wider canals than gliding or saltatorial ones (Pfaff et al. 2017), otters and minks have more elliptical anterior SCCs than non-aquatic musteloids (Grohé et al. 2016), and primates with faster head rotations have more orthogonally oriented SCCs (Malinzak et al. 2012). Comparative analysis of the SCCs has even become a tool to infer the locomotory behaviour of extinct animals and to assess phylogenetic relationships (e.g. Bhagat et al. 2021; Urciuoli et al. 2021; Bronzati et al. 2021; Tambusso et al. 2021). Many anatomical features of the SCCs that were found in highly agile taxa (e.g. gliding, flying, or arboreal groups) have been linked to the sensory requirements of their lifestyles. However, the vast majority of these studies focused on the agility of animals living above the ground, and much less is known about SCC adaptations to life underground. This is remarkable, because living underground poses very specific challenges that may also require highly sensitive SCCs, irrespective of the animal's level of agility. Living in darkness, subterranean mammals cannot rely on vision for balance or navigation. Thus, for these tasks, they presumably rely more heavily on their other senses, such as the vestibular senses (Lindenlaub et al. 1995; McVean 1999). Efficient orientation is all the more important underground, because the energy cost of burrowing greatly exceeds that

of locomotion above the ground (Vleck 1979). Once burrow systems are established, subterranean mammals have to orient themselves within what is in effect a three-dimensional maze, moving not only in the horizontal plane but also in the vertical dimension (Maddin and Sherratt 2014). Blind mole rats (*Spalax ehrenbergi*) are capable of efficiently digging bypass tunnels to avoid obstacles (Kimchi and Terkel 2003), and there is anecdotal evidence that many other subterranean species may be able to do so too (Jarvis and Sale 1971; Brett 1991; Kimchi and Terkel 2001, 2003; Kimchi et al. 2004). Homing and tunnel obstacle experiments have demonstrated the excellent spatial orientation capabilities and the apparent use of cognitive maps in various subterranean mammals, including moles and mole rats (Kimchi and Terkel 2001). For example, Kimchi and colleagues investigated in detail the path integration (i.e. navigation based not on landmarks, but on continuous processing of signals generated during locomotion) of blind mole rats (Kimchi et al. 2004). For short distances, blind mole rats rely on idiothetic (self-motion) signals, similar to other rodents, dogs or humans when tested in darkness (Kimchi et al. 2004). Vestibular information may be the primary source for path integration, but path integration may also be informed by proprioceptive signals. When covering longer distances, however, blind mole rats rely on the Earth's magnetic field, which is likely to be because estimation errors accumulate when using idiothetic information without an external, fixed, reference point (Kimchi et al. 2004).

Other subterranean species may use specialised senses other than the vestibular senses for navigation or orientation. Namib desert golden moles *Eremitalpa granti namibensis*, for example, appear to use enlarged middle ear ossicles to detect seismic cues caused by light winds blowing over the grass clumps containing their insect prey (Narins et al. 1997; Mason and Narins 2002; Lewis et al. 2006), and naked mole rats have arrays of vibrissa-like body hairs enabling highly accurate head reorientation towards a mechanosensory stimulus (Crish et al. 2003). Given that alternative sensory modalities like these are available, it is possible to argue that subterranean mammals may *not* necessarily require well-developed vestibular senses. Subterranean mammals move

through tunnel systems with very limited opportunities for directional changes, so their movement repertoire is rather simple (Lindenlaub et al. 1995; McVean 1999) and when it is impossible to take shortcuts, path integration is not necessary (Lindenlaub et al. 1995). Finally, visual cues are lacking in darkness, obviating the need for the vestibulo-ocular reflex to stabilise gaze (Maddin and Sherratt 2014; Capshaw et al. 2019). If, indeed, a subterranean lifestyle reduces the requirements on SCC sensitivity, this could have relaxed selective pressures on SCC structure.

In summary, there are arguments both for and against the need for elevated SCC sensitivity in subterranean mammals. The comparative anatomical evidence that is currently available is inconclusive in this regard. The southern marsupial mole (*Notoryctes typhlops*) has wider SCCs than non-subterranean marsupials (Pfaff et al. 2017)*;* bathyergid mole rats were reported to have unusually wide SCCs (Mason et al. 2016); *Cryptomys* sp. and blind mole rats have SCCs that are, relative to body mass, longer and have a wider internal diameter and a larger radius of curvature than brown rats (*Rattus norvegicus*) (Lindenlaub et al. 1995); the European mole (*Talpa europaea*) also has (absolutely) longer and wider SCCs than brown rats (McVean 1999); the greater mole rat (*Spalax microphthalmos*) and the southern marsupial mole have wider SCCs than aerial and arboreal members of the squirrel-related clade, while the European mole has not (Pfaff et al. 2015); and, finally, subterranean mammals belonging to the Chrysochloridae, Talpidae, Tenrecidae, and Marsupialia were not consistently found to have enlarged semicircular canals compared with non-subterranean species (Crumpton et al. 2015). Although a high internal diameter of the SCCs (wide canals) is a recurring observation, these reports typically lack phylogenetically informed statistics (Lindenlaub et al. 1995; McVean 1999; Crumpton et al. 2015; Mason et al. 2016), and those studies that do include evolutionary history in their analyses show a moderate to strong phylogenetic signal (Pagel's lambda close to one; Pfaff et al. 2015, 2017). The studies that estimated SCC sensitivity using simple equations found that *Cryptomys* sp. mole rats, blind mole rats (Lindenlaub et al. 1995) and European moles (McVean 1999) have significantly more sensitive SCCs than brown rats; that the European mole and the southern marsupial mole have a low to average SCC sensitivity compared to non-subterranean members of the squirrel-related clade, and that the greater mole rat has a rather high SCC sensitivity compared to other members of the same group, but only for the posterior SCC (not for the anterior SCC; Pfaff et al. 2015).

In this study, we test the hypothesis that the form and function of SCCs evolved in parallel in distinct lineages of subterranean mammals. To do so, we first compiled SCC size and width measurements from a large number of mammalian species with distinct lifestyles, including

subterranean and non-subterranean species. Next, the sensitivities of SCCs of different widths were estimated using fluid–structure interaction (FSI) modelling to assess how morphological variation relates to functional variation. Lastly, we used phylogenetic comparative methods to test for parallel evolution in SCC form and sensitivity, in species occupying similar ecological habitats.

Materials and methods

Ear morphology

We gathered a large dataset of SCC measurements by combining data from the literature, measurements from newly made μCT scans, and measurements from μCT scans that were already available.

Own measurements

We obtained the heads of five naked mole rats (*Heterocephalus glaber*; 4 males and 1 female) which had been euthanised for the purposes of other studies. These naked mole rats were 4–40 months old (the vestibular system reaches its final size in the early foetal stages; Costeur et al. 2017). Naked mole rats were bred in-house and maintained in an interconnected network of cages in a humidified (~ 55%) temperature-controlled room (28 °C) with red lighting (08:00–16:00), and had access to food ad libitum. In addition, a heat cable provided extra warmth under 2–3 cages/colony. Naked mole rats were killed by CO_2 exposure followed by decapitation. Experiments were conducted under the Animals (Scientific Procedures) Act 1986 Amendment Regulations 2012 under a Project Licence (P7EBFC1B1) granted to E. St. J. Smith by the Home Office and approved by the University of Cambridge Animal Welfare Ethical Review Body. The basicranium was dissected out and fixed in 4% neutrally buffered formaldehyde (Sigma-Aldrich, St. Louis, USA). We stained the samples in a 2.5% phosphotungstic acid solution in water (PTA; Merck, Darmstadt, Germany) for three weeks, in order to enhance the soft tissue contrast (Buytaert et al. 2014). After staining, each sample was rigidly mounted in a sample holder using a 6% agar solution, and μCT scanned in a Skyscan 1172 μCT scanner (Bruker, Kontich, Belgium) to visualise the vestibular system. For a list of the scan parameters, see supplementary table S1.

In addition to the aforementioned five specimens, we used CT scans of the ear regions of a further four adult or near-adult naked mole rats from the same colony (aged between 4 and 65 months old), which had been made as part of a previous study (Mason et al. 2016). Heads of three specimens from a different colony, stained with iodine, had been obtained from Dr Phil Cox: one ear

region from each of these mole rats were also scanned, as was the ear region of one laboratory mouse (*Mus musculus*) and the whole head of a second mouse. Preservation does not affect the size or shape of the bony labyrinth (Buytaert et al. 2014). They were all scanned in a Nikon XT H 225 scanner using similar settings (see supplementary table S1 for details).

All tomograms were segmented in the commercial 3D image processing software Amira (v. 5.4.4; FEI, Hillsboro, USA), using a combination of automatic thresholding based on the grey-scale value of the pixels and manual corrections in the three orthogonal views. Next, we converted the segmentation into a 3D surface model of the bony labyrinth, from which we measured the diameter of the annulus created by each canal (D) and the internal width (diameter) of the canal (d) following a similar measuring protocol to that proposed by Pfaff et al. (2015) (Fig. 1). The diameter of the annulus was measured in two directions: from the surface of the vestibule (for the anterior and horizontal canal) or the common crus (for the posterior canal) to the opposite (inner) wall of the bony canal (D_1), and from inner wall to inner wall in the perpendicular direction (D_2; Fig. 1). We measured D_1 and D_2 in three locations, approximately equally spaced within the annulus (see Fig. 1), and used the maximal diameters for further calculations. We measured the internal widths of each canal at 25%, 50%, and 75% of the length of the slender part of the canal (Fig. 1), and the average internal width of the canal (d) was calculated.

Next, we calculated the radius of curvature (R; the distance from the centre of the annulus to the centre of the canal) and the relative width of each canal:

$$R = \frac{1}{2} \cdot \left(\frac{D_1 + D_2}{2} + d \right), \tag{1}$$

$$\text{relative canal width} = \frac{d}{2R}. \tag{2}$$

All measurements described above are based on the bony labyrinth. The anatomy of the membranous labyrinth is only rarely investigated in comparative studies of the inner ear, presumably because it is extremely challenging to properly visualise its very thin walls (10–50 μm) using μCT scanning (Goyens et al. 2019). Nevertheless, the membranous labyrinth walls were clearly visible on three of the scans that we made of *H. glaber*. Hence, we segmented the membranous labyrinths on these scans in the same way as we segmented the bony labyrinths. The width of the membranous labyrinth (d_{duct}) was on average (± SD) 71% (± 6.4%) of the width of the bony labyrinth (d) for these three specimens. Because the proportionality between the width of the bony and the membranous

labyrinth is unknown for most of the other species considered here, we used this percentage to estimate the width of the membranous labyrinth of all other specimens for the sensitivity calculations.

Literature data

We searched the literature and online databases for measurements of the bony labyrinths of subterranean mammals. We also added the non-subterranean taxa that were included in the same studies to our database; these were usually taxa that were phylogenetically related to the subterranean species. In this way, we collected morphological data on the bony labyrinth of 100 individuals from 90 species, belonging to 85 mammal genera (22 families and 10 orders) (Table S2; Lindenlaub and Oelschläger 1999; McVean 1999; Pfaff et al. 2015, 2017; Crumpton et al. 2015; Mason et al. 2016; Lihong et al. 2016) and Morphosource reference numbers 000114562 and 000081856. In total, this study contains 91 species, as our own measurements included one species (*Mus musculus*) that was not present in the literature datasets that we used. We noted minor discrepancies in measuring protocols among studies: Lindenlaub and Oelschläger (1999) and McVean (1999) did not specify how they measured D, and Mason et al. (2016) and Crumpton et al. (2015) used a different definition of D (to the centre of the canal). We recorded canal radius of curvature (R), internal canal width (d), and canal type (anterior, posterior, horizontal). Data were collected from between one and four individuals per species. Species were categorised into one of two ecological classes based on the habitat they use: (1) "subterranean" species spend considerable parts of their lives within elaborate tunnel systems, excluding species that use simple burrows as refuges, and (2) "non-subterranean" species living aboveground. The latter category was further subdivided into "arboreal" species that live or spend substantial time in tree canopies, "gliding" species that travel frequently through the air, "terrestrial" species that mainly live on the ground, and "semi-aquatic" species that spend part of their time on land and part in water. The sex of the specimens was usually not provided by the literature sources.

Sensitivity calculations

We used fluid–structure interaction (FSI) models to investigate the influence of the relative canal width and radius of curvature on the absolute sensitivity of the SCCs, taken to be proportional to the strain on the cupula (see below; "Solid model" section). Compared to analytical models, FSI modelling allows explicit modelling of the cupula, inclusion of almost any membranous labyrinth anatomy, and checking flow patterns and pressure distributions at any location within the ducts (Goyens et al. 2019). The FSI model

calculates the endolymph fluid flow in the SCCs during a head manoeuvre, the cupular sensor deformation, as well as the interaction between both. A detailed description of the FSI model, its convergence analysis, sensitivity analysis, and validation are given by Goyens et al. (2019) and Goyens (2020). This investigation uses a reductionist approach, in which we keep all parameters constant across all species, except for the relative canal width and the radius of curvature. In reality, many other parameters differ among species as well (e.g. the proportionality of the membranous and osseous parts, the ampulla size, the ellipticity of the canal, and the angular accelerations of the head). Whether these other parameters differ significantly between subterranean and non-subterranean mammals is unknown, and the reductionist approach enables us to focus on the functional consequences of relative canal width and radius of curvature in a comprehensive way. We investigate two sets of models. In the first model set, we keep all parameters constant (see below), except for the relative canal width. The outcomes of these models show the size-normalised effect of relative canal width on sensitivity. In the second set of models, we vary both the relative canal width and the radius of curvature (while keeping all other parameters constant), resulting in absolute sensitivity values (i.e. sensitivities that take size into account).

Geometry

The geometry of the FSI model comprises a simplified version of the membranous labyrinth described by Curthoys and Oman (1987). It consists of a single, circular duct with a circular cross section and a wider chamber, representing the ampulla (Fig. 2), and was constructed in Ansys Designmodeler (Ansys 2019 R2; Pittsburgh, USA). We favoured modelling single ducts over a system containing three interconnected ducts (1) to reduce construction and calculation time and (2) because the SCCs are functionally separated in most situations, despite their morphological connection (Muller and Verhagen 2002). The relative canal width was varied by changing the width of the duct (maintaining a constant ampulla size), and the radius of curvature was varied by scaling the entire model. For the absolute sensitivity calculations, we simulated 25 combinations of radii of curvature and relative canal widths (Supplementary table S3) to calculate a functional landscape (see "Absolute sensitivity"). To evaluate the effect of relative canal width itself, we focused on ten models with a range of different internal canal widths but constant radii of curvature (Supplementary table S3). The disk-shaped cupula in the centre of the ampulla was 0.22 times as thick as the height of the ampulla. The shape of the crista was taken to be 0.24 times the height of the ampulla (Fig. 2).

Mesh

We created a tetrahedral mesh for the solid (cupula) and fluid parts in Ansys Meshing (Ansys 2019 R2; Pittsburgh, USA). We varied the maximal edge length according to the model's size, arriving at 14–16k elements in the cupula and 500–600k elements for the fluid.

Head manoeuvre

The canals were excited by a rotation of 0.52 rad (30°) from start to stop around their centre in 0.222 s. This manoeuvre
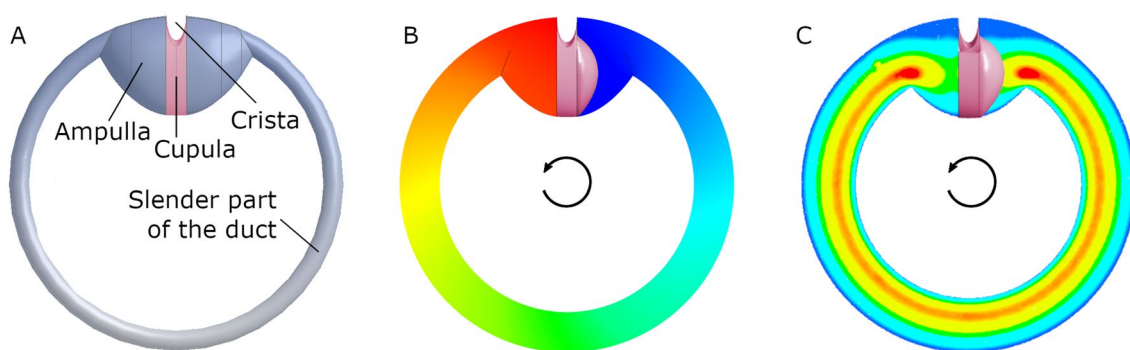

Fig. 2 Examples of FSI models with different relative canal widths (increasing width from **A**–**C**). **A** The average relative canal width of non-subterranean mammals (0.092; e.g. found in the laboratory mouse *Mus musculus*, the Cape ground squirrel *Geosciurus inauris* and the Siberian chipmunk *Eutamias sibiricus*). **B** Relative canal width of 0.2 (e.g. found in the southern marsupial mole *Notoryctes typhlops* and the greater mole rat *Spalax microphthalmus*). **C** Relative canal width of 0.3 (e.g. found in the naked mole rat *Heterocepha*-*lus glaber*). The simulated and depicted canals refer to the membranous labyrinth, but the relative canal width values are given for the bony labyrinth. In **A**, the cupula is depicted in pink, the endolymph in blue-grey. **B** The endolymph pressure at $t = 0.11$ s, ranging from 0 to 0.66 Pa, and **C** shows the relative endolymph velocity at $t = 0.11$ s, ranging from 0 to 0.00035 m/s. The arrow in **B** and **C** indicates the direction of the head manoeuvre; the deformation of the cupula is enlarged for visibility

is based on measurements of natural human movements and reaches a top velocity of 4.4 rad/s (250°/s) at 0.111 s (Carriot et al. 2014, 2017; Goyens 2019).

Fluid model

We modelled the dynamics of the endolymph fluid inside the canal using CFD in Ansys Fluent (Ansys 2019 R2; Pittsburgh, USA). Because of the low Reynolds number (Muller 1999), we used a laminar viscous flow model (Goyens et al. 2019). We implemented a fluid density of 998.2 kg m^{-3} and a dynamic viscosity of 8.5×10^{-4} Pa s because the fluid properties of endolymph are known to resemble those of water—investigated in human and cat by Steer et al. (1967). The walls were modelled as 'no slip' surfaces. The head manoeuvre was implemented with a 'User-Defined Function' for frame motion using the 'Define Zone Motion' macro.

Solid model

We modelled the cupular deformation using FEM in Ansys Transient Structural. The cupula adheres to the ampulla walls along its entire circumference. Therefore, these walls rotate along with the head manoeuvre, which we defined by a function. Consistent with the literature, we used a Young's modulus of 54 Pa, a Poisson ratio of 0.3, and a density of 998.2 kg m^{-3} for the cupula (Steer et al. 1967; Kassemi et al. 2005; Obrist 2011). The hair cells that generate an afferent signal when deflected are located at the crista surface. Hence, we calculated the maximal strain in the cupula at the crista surface (where the hair cells are located; Fig. 2A), as a measure for the excitation of the canal. Because all models are stimulated by the same head manoeuvre, we used this as the measure for the sensitivity of the canal.

Interaction between endolymph and cupula

The System Coupling module of Ansys Workbench (Ansys 2019 R2; Pittsburgh, USA) governs the two-way interaction between the fluid part (endolymph) and the solid part (cupula) of the model. Forces exerted by the endolymph on the cupula are transferred from Ansys Fluent to Ansys Transient Structural, and the resulting cupula deformation is transferred from Ansys Transient Structural to Ansys Fluent. We enabled dynamic remeshing in Ansys Fluent to deal with these changes of the interaction surface during the simulation.

Absolute sensitivity

We fitted a cubic polynomial surface using the least-squares method through the maximal strain values (i.e. sensitivity) of the 25 combinations of radius of curvature and relative canal width to capture the functional landscape ($R^2 = 0.97$; mean squared error $= 1.4 \times 10^{-4}$). Next, we evaluated this surface fit for the combination of parameter values of each of the specimens in our dataset, to estimate their absolute sensitivity. We used the estimations of the internal width of the membranous labyrinth ducts for this purpose, because the functional body of fluid that excites the SCCs is contained inside the membranous labyrinth (i.e. we multiplied d by 0.71).

Phylogenetic comparative statistics

All data were statistically analysed in R (version 3.6). To test whether relative canal width and absolute ear sensitivity vary among species occupying different environments, we used Monte Carlo Markov chain generalised linear mixed models (*MCMCglmm* v2.29 package (Hadfield 2010)), as this enables the inclusion of a phylogenetic structure in a Bayesian generalised linear modelling framework (Hadfield 2010; Hadfield and Nakagawa 2010). The recent mammalian phylogenetic tree proposed by Upham et al. (2019) was pruned to include only the 91 species considered in this study. Ten species for which we amassed ear morphology data were not represented in the Upham tree, but we used the phylogenetic position of the most closely-related congeneric species for our phylogenetic comparative analyses (Table S2). For the purposes of model fitting, we first performed a preliminary test to explore whether variation in relative canal width (response variable) could be explained by species' habitat use and to test whether relative canal width differs among canal types. Here, we included 'habitat' (four-level factor: arboreal, gliding, subterranean, terrestrial) and 'canal type' (three-level factor: anterior, horizontal, posterior) as fixed effects. Four species (*Condylura cristata, Galemys pyrenaicus, Limnogale mergulus, Potamogale velox*) were excluded from this particular model, as they are generally labelled as 'semi-aquatic' and therefore did not clearly fit one of the four aforementioned habitat categories. We used Gaussian models with 'phylogeny' and 'individual' (nested in 'species') as random effects. In a second model, we pooled all arboreal, gliding, terrestrial, and semi-aquatic species in one category (i.e. 'non-subterranean') and tested whether relative canal width differs between subterranean and non-subterranean species, for each canal type. Fixed and random effects were identical to the first model, apart from that this second model incorporated the interaction between the two fixed effects. Random effects were identical in the first and second models. Lastly, we tested whether absolute ear sensitivity differs between subterranean and non-subterranean species (fixed and random effects were identical to the second model). In all models, we used an inverse-Wishart prior ($V = 1$, $v = 0.002$) for both the residual term and the random effect. Each model was run for 5,000,000 iterations with a

1000 burn-in (as in e.g. Baeckens et al. 2021). Chains were sampled every 500 iterations. Aside from the 2019 course notes by Jarrod Hadfield, model parameters were chosen based on Hadfield (2010) and Garamszegi (2014). From the models, we calculated the mean and 95% credible interval (CI) for the intercept (β).

To investigate whether and how changes in habitat use have influenced SCC morphology and sensitivity, we used a model selection framework. These models are each limited to the analysis of just one canal type, so species averages of relative canal width and absolute ear sensitivity were calculated for each canal type separately. Here, we are particularly interested in those canal types that our preceding Bayesian generalised linear models indicated as varying among subterranean and non-subterranean species. We tested three different models of evolution using the methods and codes (*ouch* v2.14 package) developed by Butler and King (2004). Out of the three models, the first model tested whether the trait of interest varies at random following a Brownian motion (BM) process, where phenotypic variation accumulates with time. A rejection of the BM model implies that phenotypic evolution has not followed a random evolutionary trajectory (neutral drift). The two other models followed an Ornstein–Uhlenbeck (OU) process (Lande 1975; Hansen 1997; Cressler et al. 2015), with the simplest model ('OU1') having a single optimal for all species regardless of selective regime. A third model ('OU2') adds additional optima for each selective regime so that we have separate optima for the two different habitat types (i.e. subterranean and non-subterranean) by estimating an ancestral regime optimum for all internal branches (based on maximum likelihood). To determine the goodness of fit of candidate evolutionary models, we compared the likelihood of the models by means of a χ^2 test (as in e.g. Baeckens et al. 2020).

Results

Canal size diversity and evolution

The radii of curvature (R) of the SCCs for the species in our study ranged between 639 and 5000 µm. Phylogenetic Bayesian generalised linear mixed models show no significant differences in radius of curvature between subterranean and non-subterranean mammal species (anterior: $\beta = -0.390$, CI = [−1122, 288]; posterior: $\beta = -260$, CI = [−0.964, 473]; horizontal: $\beta = -216$, CI = [−938, 492], all pMCMC ≥ 0.276). The relative width ($d/2R$) of the three ear canals varies considerably among species inhabiting different environments, however (Fig. 3A). Our models indicate that relative canal widths of subterranean species are significantly larger in comparison to arboreal (anterior: $\beta = -0.072$, CI = [−0.102, −0.040]; posterior:

$\beta = -0.072$, CI = [−0.103, −0.041]; horizontal: $\beta = -0.072$, CI = [−0.103, −0.040], all pMCMC < 0.001), gliding (anterior: $\beta = -0.068$, CI = [−0.103, −0.030]; posterior: $\beta = -0.068$, CI = [−0.106, −0.033]; horizontal: $\beta = -0.068$, CI = [−0.106, −0.032], all pMCMC < 0.001), and terrestrial species (anterior: $\beta = -0.055$, CI = [−0.084, −0.027]; posterior: $\beta = -0.056$, CI = [−0.084, −0.026]; horizontal: $\beta = -0.056$, CI = [−0.083, −0.27], all pMCMC < 0.001; Fig. 3B). Within the subterranean mammals, the bathyergid mole rats have particularly wide canals relative to radius of curvature (Fig. 3A).

Lumping all non-subterranean species into one category, we continue to see the substantial difference in relative canal width between subterranean and non-subterranean species, but we also observe significant variation among canal types. Bayesian estimates of mean [CI] relative canal width in subterranean species ranged from 0.134 [0.080, 0.185] in the anterior canal, to the significantly larger posterior and horizontal canals of 0.174 [0.120, 0.226] ($\beta = 0.039$, CI = [0.029, 0.050], pMCMC < 0.001) and 0.181 [0.117, 0.242] ($\beta = 0.046$, CI = [0.036, 0.057], pMCMC < 0.001), respectively. The relative widths of the latter two canals, however, do not differ significantly from each other ($\beta = 0.007$, CI = [−0.003, 0.030], pMCMC = 0.183). The anterior canal is also the narrowest of all three canals in non-subterranean species, with a relative canal width of 0.083 [0.034, 0.132] that is significantly lower than the value of 0.105 [0.056, 0.157] for the posterior canal ($\beta = 0.022$, CI = [0.016, 0.028], pMCMC < 0.001), which is again significantly lower than the value of 0.122 [0.021, 0.225] for the horizontal canal ($\beta = 0.039$, CI = [0.034, 0.046], pMCMC < 0.001).

Our analyses also indicate that the differences in relative canal width between subterranean and non-subterranean species vary among canal types (Fig. 3C). Specifically, the difference in relative canal width between subterranean and non-subterranean species is most pronounced in the posterior canal and least in the anterior canal, and differs significantly between the posterior and anterior canals (interaction: $\beta = 0.018$, CI = [0.006, −0.030], pMCMC = 0.004). The difference in relative horizontal canal width between subterranean and non-subterranean species does not vary significantly from the differences in the anterior (interaction: $\beta = -0.007$, CI = [−0.019, 0.004], pMCMC = 0.252) and posterior canals (interaction: $\beta = 0.011$, CI = [−0.001, 0.023], pMCMC = 0.063).

To examine the potential adaptive evolution of relative canal width, we tested three different models of evolution. The overall fit of each of the three evolutionary models is summarised in Table 1. Both OU models were tested against BM, which showed that the best-fitting model, for all three canal types, was the adaptive model OU2; the worst-fitting model was not BM but the 'wrong' adaptive model, OU1. The parameter estimates of the best-fitting
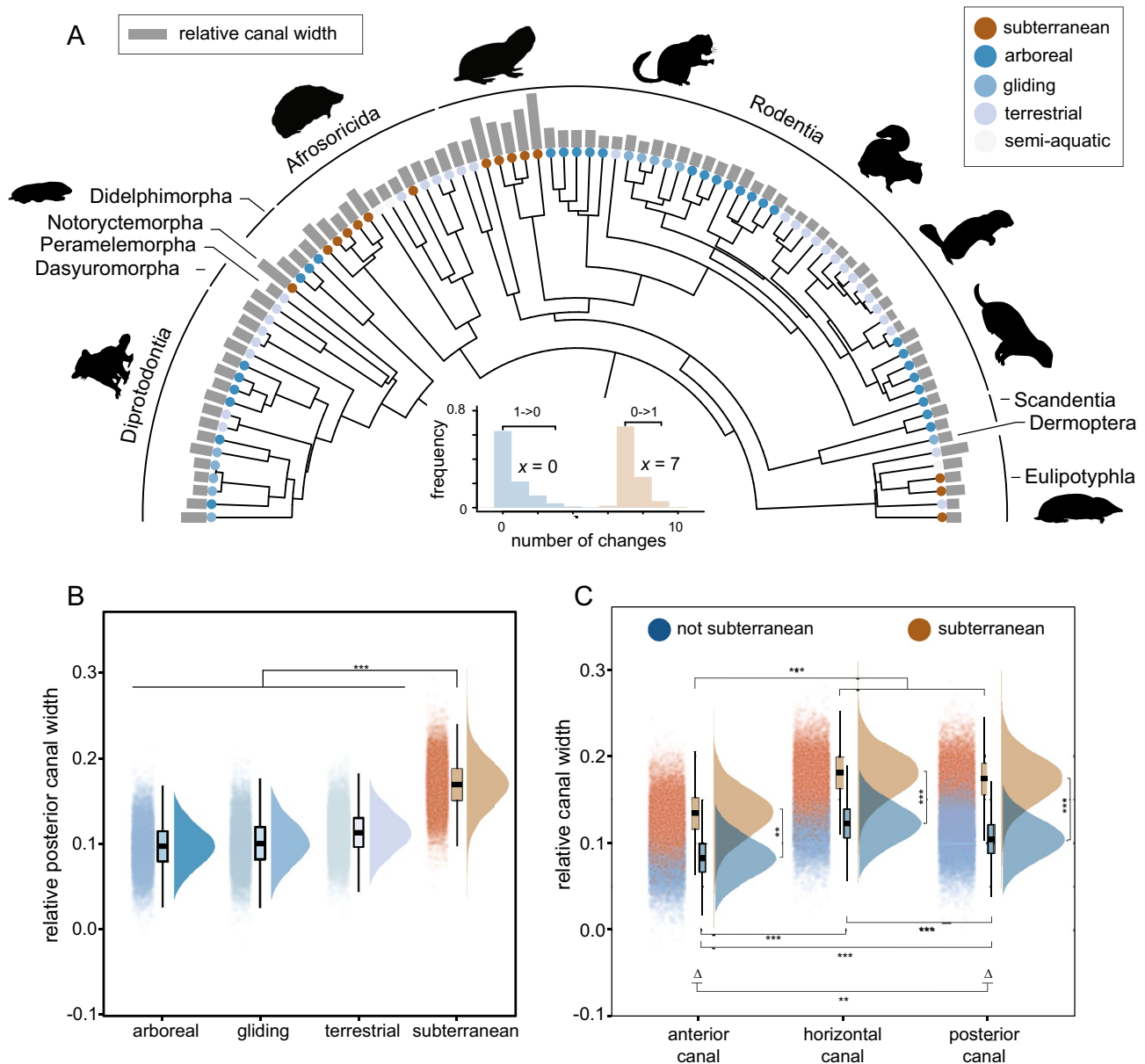
Fig. 3 Evolution of relative canal width. **A** Phylogenetic relationships of the 91 species studied, with the coloured circles at the tree tips representing species' habitat use. Bars at the tree tips denote species' relative canal width of the posterior canal. The density plot at the root of the tree illustrates the estimated number of transitions (*x*) from a subterranean ('1') to a non-subterranean ('0') lifestyle along the evolutionary history in blue, and from a non-subterranean to a subterranean lifestyle in pink [calculated using 'density.multiSimmap'

function in *phytools* (Revell 2012)]. The Bayesian model predictions [as raincloud plot (Allen et al. 2019), boxplot, and posterior distribution] for relative canal width show (**B**) the differences among species with distinct lifestyles (the same colours as in **A** and **C** the differences between subterranean and non-subterranean species per canal type. Asterisks denote level of statistical significance (***< 0.001; **< 0.01)

model, OU2, suggested strong selection (*α* ranged between 0.99 and 1.90) with moderate drift (*σ* ranged from 0.004 to 0.006; comparable to that estimated for the BM model for which *σ* ranged from 0.003 to 0.005). Together, these results suggest that relative canal width oscillates around

two phenotypic optima, one for each of the different selective regimes, i.e. subterranean and non-subterranean.

Table 1 Performance of models of relative canal width evolution

Canal type	Model	LogL	AICc	χ^2	*P* value
Anterior	BM	207	−410		
	OU(1)	207	−407	0.60	0.896
	OU(2)	**212**	**−416**	**9.83**	**0.043**
Horizontal	BM	180	−356		
	OU(1)	180	−352	0.97	0.809
	OU(2)	**190**	**−371**	**18.96**	**< 0.001**
Posterior	BM	186	−368		
	OU(1)	185	−363	3.04	0.385
	OU(2)	**205**	**−402**	**38.12**	**< 0.001**

The likelihood values (LogL) and bias-corrected AICc are given for each model. The likelihood of each OU model was tested against BM using a Chi-square (χ^2) test. The best-fit model is represented in bold font

Functional implications of the relative canal width

The SCCs of the specimens in our dataset differ both in size (radius of curvature, R) and in internal canal width (d). Canals with a larger radius of curvature are predicted to be more sensitive (Oman et al. 1987; Muller 1999; Goyens 2019), and our models show that wider canals are also more sensitive (Fig. 4A, C). Considering SCCs of the same radius of curvature, there is a sigmoid-shaped relationship between relative canal width and size-normalised sensitivity (see Fig. 4A). Between relative canal widths of 0.07 and 0.20, the size-normalised sensitivity increases almost linearly; a 10% increase in relative canal width leads to a 3.85 times higher sensitivity. Above or below this range, the sensitivity rises much more slowly (Fig. 4A). It is possible to make a reasonably accurate prediction of the absolute SCC sensitivity based on the (absolute) internal canal width (d) alone (see Fig. 4C; $R^2 = 0.80$; absolute sensitivity $= 0.0002d - 0.054$). The (absolute) internal canal width (d) is a better predictor of the absolute sensitivity than the absolute radius of curvature (R; Fig. 4C, D).

Ear sensitivity diversity and evolution

The functional landscape based on FSI modelling (Fig. 4B) allows us to estimate the absolute sensitivity of all canals in our dataset, taking into account both their radius of curvature (R) and relative canal width. The absolute ear sensitivity varies significantly between non-subterranean and subterranean species, but this is only true for the anterior canal ($\beta = 0.049$, CI = [0.019, 0.078], pMCMC = 0.001), and not for the posterior ($\beta = 0.020$, CI = [− 0.009, 0.050], pMCMC = 0.186) or horizontal canals ($\beta = 0.017$, CI = [− 0.013, 0.045],

Fig. 4 Size-normalised and absolute sensitivity. **A** FSI model outcomes show the effect of the relative canal width on the size-normalised sensitivity (i.e. models with a constant radius of curvature; expressed as a percentage of the sensitivity of the model with the widest canals). **B** Functional landscape showing the combined effect of canal radius of curvature (R) and relative canal width on the absolute sensitivity (measured as the maximal strain of the cupula at the crista surface; represented by the grey-scale values). **C** Relationship between the internal canal width (d) and the absolute sensitivity. **D** Relationship between the radius of curvature (R) and the absolute sensitivity. Each coloured marker in **A** and **B** refers to one of the SCCs of the specimens in the dataset. In **B**–**D**, the anterior SCCs are indicated by stars, posterior SCCs by open circles, and horizontal SCCs by filled circles. The indicated terrestrial species in **B** is the mountain beaver *Aplodontia rufa*
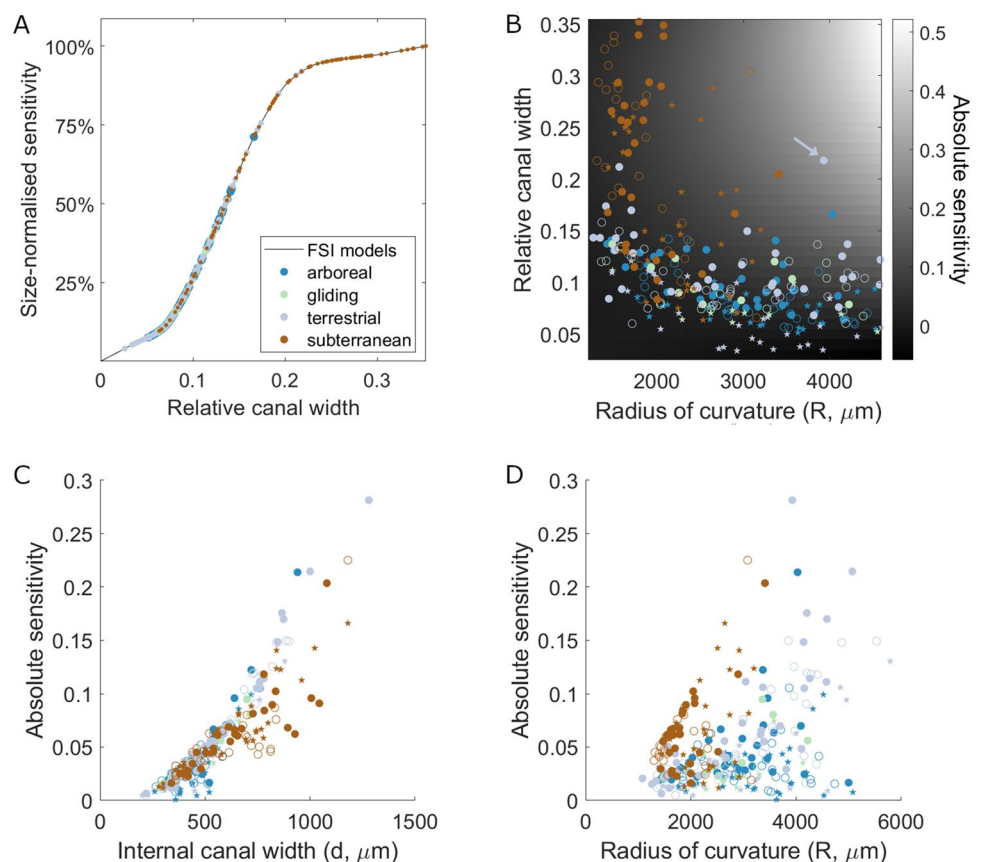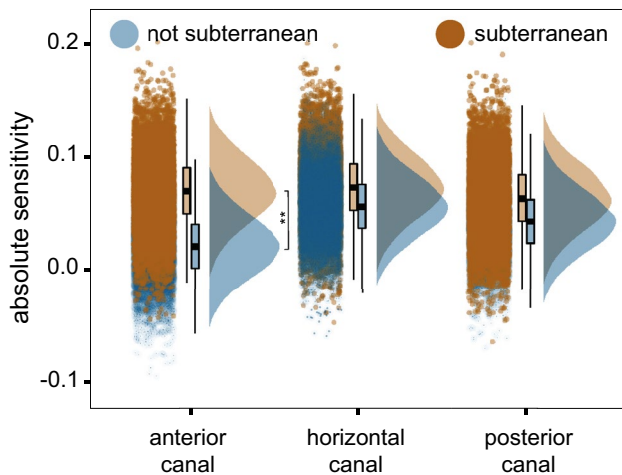
Fig. 5 Ear sensitivity variation among canal types and ecology. Bayesian model predictions (as raincloud plot (Allen et al. 2019), boxplot, and posterior distribution) for absolute ear sensitivity show a significant difference between subterranean and non-subterranean species in the anterior canal, but not in the horizontal and posterior canals

pMCMC = 0.248). More specifically, the anterior canal of subterranean species is more sensitive than that of non-subterranean species (Fig. 5). Evolutionary model selection of absolute sensitivity of the anterior canal revealed that the BM model (LogL = 194.24, AICc = − 384.34) was outperformed by both OU models (OU1, χ^2 = 8.90, P = 0.003; OU2, χ^2 = 14.25, P < 0.001), with the OU2 adaptive model (LogL = 201.37, AICc = − 394.26) showing a better fit than OU1 (LogL = 198.69, AICc = − 391.10).

Discussion

The evolution of larger and more sensitive SCCs as an adaptation to a lifestyle that requires increased balance control and navigational skills has been previously documented in highly agile and fast-moving mammals, such as gibbons and galagos (Spoor et al. 2007). In this study, we discovered that diversification of the SCCs also occurred in subterranean mammals. Specifically, we find that subterranean mammals considered collectively have evolved a larger relative canal width than their non-subterranean relatives. For the anterior canal only, this leads to a significant increase in SCC sensitivity in subterranean mammals. This may seem surprising, given that the difference in the relative canal width between subterranean and non-subterranean mammals is actually the smallest for the anterior SCC (Fig. 3C). The reason is that the non-linear interplay between the relative canal width (significant differences) and the radius of curvature (no significant differences) together determine the absolute

sensitivity, and lift the difference above the level of significance for the anterior SCC only.

When calculating sensitivities using FSI, we considered a constant proportionality between the membranous ducts and osseous canals in all species. It is noticeably, however, that the membranous ducts that we measured in naked mole rats seem to be proportionally wider relative to the bony canals (71% on average) than in non-subterranean mammals—see e.g. Figure 2 in David et al. (2016). If such a difference does indeed exist, this would make our results on patterns of convergence even stronger.

Ecological significance of increased relative canal width and sensitivity in subterranean mammals

Our findings show that most subterranean mammal species have relatively wider SCCs than species living above the ground. Fluid–structure interaction modelling shows that canal widening has a sensitivity-enhancing effect. The canal widening and enhanced anterior SCC sensitivity in subterranean mammals imply higher demands on navigation or balance when living underground. Experimental work, indeed, supports the notion that at least some subterranean mammals exhibit excellent navigation, bypassing, or homing skills (Kimchi and Terkel 2001, 2003; Kimchi et al. 2004; Lewis et al. 2006), but it is often not clear which sensory organs are responsible for these abilities. Our findings of canal widening and associated sensitivity enhancement in subterranean mammals strongly suggest that the vestibular system plays an important role in navigation and/or balance in many subterranean mammals. Future experimental research (e.g. suppressing SCC sensitivity) may elucidate the functional role of SCC sensitivity in the navigation and balance of these burrowing animals.

Our functional landscape analysis also allows predicting the SCC sensitivity of species that are not included in our dataset (Matlab functional surface in the Supplementary Material S5). To illustrate, based on the primate dataset by Spoor et al. (2007), our models predict an anterior SCC sensitivity of ≈ 0.0134 for the Senegal bushbaby (*Galago senegalensis*, body mass = 0.220 kg), a horizontal SCC sensitivity of ≈ 0.0014 for the Guianan squirrel monkey (*Saimiri sciureus*, body mass = 0.759 kg) and a horizontal SCC sensitivity of < 0.001 for the diademed sifaka (*Propithecus diadema*, body mass = 6.1 kg) (Spoor and Zonneveld 1998; Spoor et al. 2007; Silcox et al. 2009). Surprisingly, these predictions suggest lower SCC sensitivities for these highly agile primates than for the subterranean mammals in our dataset (absolute sensitivity anterior SCC: 0.066 ± 0.040; posterior SCC: 0.056 ± 0.038; horizontal SCC: 0.064 ± 0.038). The reason for this result is that the three aforementioned primates have rather narrow SCCs (*d*: 163–264 μm) with average radii of curvature (*R*:

1633–2612 μm) compared to the mammals in our dataset. Hence, our findings suggest that it would be worth collecting internal width measurements as well as measurements of the radius of curvature in future comparative research on the vestibular system.

One possible functional explanation for lower absolute sensitivities in these primates than in subterranean mammals relates to differences in their commonly deployed angular frequency range of head movements. Canal widening improves the sensitivity (Fig. 4A, C), but at the same time, probably increases the time required for the canal to respond to a stimulus (Muller 1999). To the best of our knowledge, no comparative studies have been published on angular head frequencies, but it is likely that subterranean mammals, which tend to carry massive neck and/or shoulder musculature associated with digging, move their heads more slowly than primates. If so, a slower SCC response may not hamper subterranean mammals due to their slower head movements. In contrast, highly agile animals may stimulate their narrow, less sensitive SCCs more strongly with high head accelerations while benefiting from a faster response time. We encourage future studies to examine the functional trade-off between SCC sensitivity and response time across animal groups with distinct locomotion styles.

Repeated evolution of SCC form and function

Similarities in animal form and function associated with particular habitats can provide strong evidence for adaptive evolution by natural selection (Losos and Miles 1994; Larson and Losos 1996; Losos 2011). We showed that the vestibular system of subterranean mammal species is characterised by relatively wider SCCs with a higher sensitivity of the anterior SCC in comparison to closely-related, non-subterranean species. Moreover, our results revealed repeated evolution of this SCC form and performance associated with the independent transitions to a subterranean lifestyle.

Our results allow us to make predictions about the lifestyle (i.e. subterranean or not) of mammalian species based only on their vestibular anatomy. Based on Bayes' theorem, we can calculate the probability that a species is subterranean using the posterior distributions in Fig. 3C. Making no a priori assumptions, there is a > 95% chance that a species is subterranean when the relative canal width of its anterior SCC ≥ 0.146, its posterior SCC ≥ 0.167, or its horizontal SCC ≥ 0.184 (see Fig. 6; average value: 0.166). Following this reasoning for the outlier in the terrestrial group indicated in Fig. 4B, we find that the mountain beaver (*Aplodontia rufa*) falls into this category. Mountain beavers dig extensive burrows,
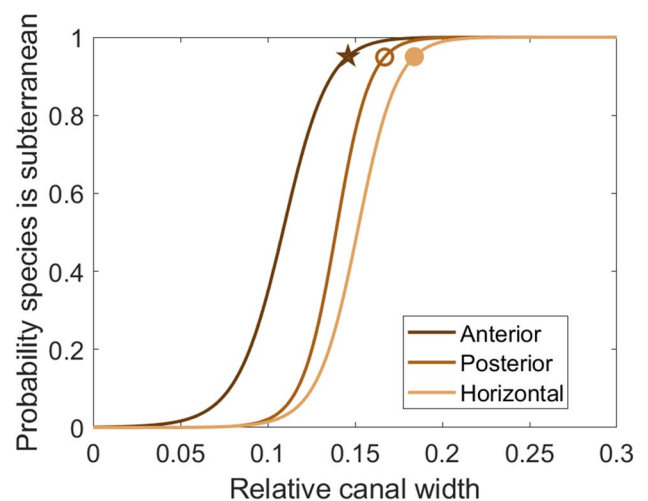

Fig. 6 Probability that a mammalian species is subterranean. The posterior distributions allow one to predict whether a mammalian species is subterranean or not, based on the relative canal width of one of its SCCs. The 95% probability is indicated for the anterior canal (star), the posterior canal (open circle), and the horizontal canal (filled circle)

rarely travel further than a few meters from their burrow entrance, have limited visual abilities, and have cochlear specialisations that were suggested to allow detection of slow air pressure changes in their burrows (Carraway and Verts 1993). It is worth noting, though, that the mountain beaver specimen in our dataset only has a high relative canal width for its horizontal SCC, and not for its anterior and posterior SCCs.

Possible reasons for enhanced anterior canal sensitivity

Our results show considerable differences in the sensitivities of the anterior canal (increased in subterranean mammals compared with non-subterranean species), but not in the sensitivities of the posterior and horizontal canals.

The ultimate reasons why the anterior canal alone acquires this higher sensitivity in subterranean species remain unclear. One possible explanation may be that because the anterior canal is oriented vertically, a more sensitive anterior canal gives a more precise measurement of head tilt up or down (Spoor et al. 1994). This may be particularly useful in the three-dimensional, subterranean world, for example to estimate tunnel inclination when aiming for connection to another tunnel, or to avoid the surface. However, the same reasoning would equally apply to the posterior canal, which is also oriented vertically (but usually neither in the sagittal nor in the transverse plane (Berlin et al. 2013). Hence, this does not elucidate why only

the anterior canal became more sensitive in subterranean mammals.

One characteristic that is unique to the anterior canal relates to the subarcuate fossa, a cavity lying between the three SCCs that contains cerebellar neural tissue. This tissue is connected to the rest of the cerebellum by myelinated pathways that run through the arc of the anterior canal, referred to as the ostium (Rodgers 2011). In rodents, the entire parafloccular cerebellum is located within the subarcuate fossa, while in primates it only contains the petrosal lobe of the paraflocculus (McClure and Daron 1971; Bertrand et al. 2018). Many mammalian species have subarcuate fossae, but certainly not all (McClure and Daron 1971; Jeffery and Spoor 2006) (see supplementary table S6 for a literature overview). Most research on the function of the petrosal lobe of the paraflocculus has been performed on non-human primates, demonstrating its involvement in the control of voluntary eye movements (both saccadic and smooth pursuit) (Zee et al. 1981; Rambold et al. 2002; Xiong and Nagao 2002; Hiramatsu et al. 2008; Xiong et al. 2010; Shaikh and Wang 2021). The petrosal lobe's important role in gaze stability during running led researchers to hypothesise that the size of the subarcuate fossa and the petrosal lobe may be directly associated with a species' locomotor agility (Jeffery and Spoor 2006; Jeffery et al. 2008; Rodgers 2011). The size of the subarcuate fossa is spatially related to SCC size (Jeffery and Spoor 2006), especially the anterior canal that surrounds its ostium. Jeffery et al. showed that subarcuate fossa size is unlikely to be the underlying reason for the previously observed link between canal size and agility in primates (Jeffery et al. 2008), but there is a significant positive correlation between subarcuate fossa size and the overall size of the anterior canal in primates (Jeffery and Spoor 2006; Jeffery et al. 2008).

These observations suggest a possible explanation for the relatively wide anterior canal of subterranean mammals. In their dark burrow systems, the petrosal lobe that coordinates eye movements may have lost its main function, allowing for an evolutionary shrinkage of the subarcuate fossa. This would have permitted widening of the anterior canal towards the inside, narrowing the ostium. This idea is compatible with our finding that subterranean and non-subterranean mammals have no statistically different SCC radii of curvature, suggesting that the SCCs of subterranean mammals have widened inwards as much as outwards.

Although we have considered subterranean mammals collectively so far in this discussion, it is important to recognise that there is considerable anatomical variation in the vestibular region between groups. For example, the naked mole rat *Heterocephalus* has relatively wide SCCs, the space between them being occupied by a diverticulum of the middle ear cavity (Mason et al. 2016), while the European mole *Talpa* has relatively narrower SCCs surrounding

a sizeable subarcuate fossa (Wilkie 1925). Whether or not there actually was any reduction in volume of the subarcuate fossa, which might have allowed for canal expansion, would need to be examined separately in the various subterranean groups.

Declarations

References

Allen M, Poggiali D, Whitaker K et al (2019) Raincloud plots: a multiplatform tool for robust data visualization. Wellcome Open Res 4:63

Angelaki DE, Cullen KE (2008) Vestibular system: the many facets of a multimodal sense. Annu Rev Neurosci 31:125–150

Baeckens S, Goeyers C, Van Damme R (2020) Convergent evolution of claw shape in a transcontinental lizard radiation. Integr Comp Biol 60:10–23

Baeckens S, Temmerman M, Gorb SN et al (2021) Convergent evolution of skin surface microarchitecture and increased skin hydrophobicity in semi-aquatic anole lizards. J Exp Biol 225:jeb242939

Berlin JC, Kirk EC, Rowe TB (2013) Functional implications of ubiquitous semicircular canal non-orthogonality in mammals. PLoS ONE 8:24–26

Bertrand OC, Amador-Mughal F, Lang MM, Silcox MT (2018) Virtual endocasts of fossil Sciuroidea: brain size reduction in the evolution of fossoriality. Palaeontology 61:919–948

Bhagat R, Bertrand OC, Silcox MT (2021) Evolution of arboreality and fossoriality in squirrels and aplodontid rodents: Insights from the semicircular canals of fossil rodents. J Anat 238:96–112

Billet G, Hautier L, Asher RJ et al (2012) High morphological variation of vestibular system accompanies slow and infrequent locomotion in three-toed sloths. Proc R Soc B Biol Sci 279:3932–3939

Brett RA (1991) The ecology of naked mole-rat colonies: burrowing, food, and limiting factors. Princeton University Press, Princeton

Bronzati M, Benson RBJ, Evers SW et al (2021) Deep evolutionary diversification of semicircular canals in archosaurs. Curr Biol 31:2520–2529

Butler M, King A (2004) Phylogenetic comparative analysis: a modeling approach for adaptive evolution. Am Nat 164:683

Buytaert J, Goyens J, De Greef D et al (2014) Volume shrinkage of bone, brain and muscle tissue in sample preparation for micro-CT and light sheet fluorescence microscopy (LSFM). Microsc Microanal 20:1208–1217

Capshaw G, Soares D, Carr CE (2019) Bony labyrinth morphometry reveals hidden diversity in lungless salamanders (Family Plethodontidae): structural correlates of ecology, development, and vision in the inner ear. Evolution 73:2135–2150

Carraway LN, Verts BJ (1993) Aplodontia rufa. Mamm Species 431:1–10

Carriot J, Jamali M, Chacron MJ, Cullen KE (2014) Statistics of the vestibular input experienced during natural self-motion: implications for neural processing. J Neurosci 34:8347–8357

Carriot J, Jamali M, Cullen KE, Chacron MJ (2017) Envelope statistics of self-motion signals experienced by human subjects during everyday activities: implications for vestibular processing. PLoS ONE 12:e0178664

Cherng RJ, Chen JJ, Su FC (2001) Vestibular system in performance of standing balance of children and young adults under altered sensory conditions. Percept Mot Skills 92:1167–1179

Costeur L, Mennecart B, Müller B, Schulz G (2017) Prenatal growth stages show the development of the ruminant bony labyrinth and petrosal bone. J Anat 230:347–353

Cressler CE, Butler MA, King AA (2015) Detecting adaptive evolution in phylogenetic comparative analysis using the Ornstein–Uhlenbeck model. Syst Biol 64:953–968

Crish SD, Rice FL, Park TJ, Comer CM (2003) Somatosensory organization and behavior in naked mole-rats I: vibrissa-like body hairs comprise a sensory array that mediates orientation to tactile stimuli. Brain Behav Evol 62:141–151

Crumpton N, Kardjilov N, Asher RJ (2015) Convergence vs. specialization in the ear region of moles (mammalia). J Morphol 276:900–914

Curthoys IS, Oman CM (1987) Dimensions of the horizontal semicircular duct, ampulla and utricle in the human. Acta Otolaryngol 103:254–261

David R, Stoessel A, Berthoz A et al (2016) Assessing morphology and function of the semicircular duct system: introducing new in-situ visualization and software toolbox. Sci Rep 6:32772

Ekdale EG (2016) Form and function of the mammalian inner ear. J Anat 228:324–337

Fitzpatrick RC, Day BL (2004) Probing the human vestibular system with galvanic stimulation. J Appl Physiol 96:2301–2316

Garamszegi LZ (2014) Modern phylogenetic comparative methods and their application in evolutionary biology: concepts and practice, 1st edn. Springer, Berlin

Goyens J (2019) Highly elliptical semi-circular canals reduce sensitivity to head rotation in squamates compared to mammals. Sci Rep 9:16428

Goyens J (2020) Modelling shows that stimulation of the semicircular canals depends on the rotation centre. Hear Res 396:108071

Goyens J, Aerts P (2019) Why the semicircular canals are not stimulated by linear accelerations. Bioinspir Biomim 14:056004

Goyens J, Pourquie M, Poelma C, Westerweel J (2019) Asymmetric cupula displacement due to endolymph vortex in the human semicircular canal. Biomech Model Mechanobiol 18:1577–1590

Gray AA (1907) The labyrinth of animals, Including mammals, birds, reptiles and amphibians. J. & A. Churchill, London

Grohé C, Tseng ZJ, Lebrun R et al (2016) Bony labyrinth shape variation in extant Carnivora: a case study of Musteloidea. J Anat 228:366–383

Hadfield JD (2010) MCMCglmm: MCMC methods for multi-response GLMMs in R. J Stat Softw 33:1–22

Hadfield JD, Nakagawa S (2010) General quantitative genetic methods for comparative biology: Phylogenies, taxonomies and multi-trait models for continuous and categorical characters. J Evol Biol 23:494–508

Hansen TF (1997) Stabilizing selection and the comparative analysis of adaptation. Evolution 51:1341–1351

Hiramatsu T, Ohki M, Kitazawa H et al (2008) Role of primate cerebellar lobulus petrosus of paraflocculus in smooth pursuit eye movement control revealed by chemical lesion. Neurosci Res 60:250–258

Jarvis JUM, Sale JB (1971) Burrowing and burrow patterns of East African mole-rats *Tachyoryctes*, *Heliophobius* and *Heterocephalus*. J Zool 163:451–479

Jeffery N, Spoor F (2006) The primate subarcuate fossa and its relationship to the semicircular canals part I: prenatal growth. J Hum Evol 51:537–549

Jeffery N, Ryan TM, Spoor F (2008) The primate subarcuate fossa and its relationship to the semicircular canals part II: adult inter-specific variation. J Hum Evol 55:326–339

Jiang Y, Qin Y, Lu S et al (2022) Outcomes of the bionic semicircular canals support the "density hypothesis" and "circular hypothesis." Rev Sci Instrum 93:034105

Kassemi M, Deserranno D, Oas JG (2005) Fluid–structural interactions in the inner ear. Comput Struct 83:181–189

Kimchi T, Terkel J (2001) Spatial learning and memory in the blind mole-rat in comparison with the laboratory rat and Levant vole. Anim Behav 61:171–180

Kimchi T, Terkel J (2003) Mole rats (*Spalax ehrenbergi*) select bypass burrowing strategies in accordance with obstacle size. Naturwissenschaften 90:36–39

Kimchi T, Etienne AS, Terkel J (2004) A subterranean mammal uses the magnetic compass for path integration. Proc Natl Acad Sci U S A 101:1105–1109

Lande R (1975) Natural selection and random genetic drift in phenotypic evolution. Evolution 30:314–334

Larson A, Losos JB (1996) Phylogenetic systematics of adaptation. In: Rose M, Lauder GV (eds) Adaptation. Academic Press, San Diego, pp 187–220

Lewis ER, Narins PM, Jarvis JUM et al (2006) Preliminary evidence for the use of microseismic cues for navigation by the Namib golden mole. J Acoust Soc Am 119:1260

Lihong X, Heng L, Gyanwali B et al (2016) Micro-computed tomography and microdissection of the temporal bone of tree shrews. Ann Anat 208:69–77

Lindenlaub T, Oelschläger HA (1999) Morphological, morphometric, and functional differences in the vestibular organ of different breeds of the rat (*Rattus norvegicus*). Anat Rec 255:15–19

Lindenlaub T, Burda H, Nevo E (1995) Convergent evolution of the vestibular organ in the subterranean mole-rats, *Cryptomys* and *Spalax*, as compared with the aboveground rat, *Rattus*. J Morphol 224:303–311

Losos JB (2011) Convergence, adaptation, and constraint. Evolution 65:1827–1840

Losos JB, Miles DB (1994) Adaptation, constraint, and the comparative method: phylogenetic issues and methods. In: Wainwright PC, Reilly S (eds) Ecological morphology: integrative organismal biology. University Chicago Press, Chicago, pp 60–98

Maddin HC, Sherratt E (2014) Influence of fossoriality on inner ear morphology: insights from caecilian amphibians. J Anat 225:83–93

Malinzak MD, Kay RF, Hullar TE (2012) Locomotor head movements and semicircular canal morphology in primates. Proc Natl Acad Sci U S A 109:17914–17919

Mason MJ, Narins PM (2002) Seismic sensitivity in the desert golden mole (*Eremitalpa granti*): a review. J Comp Psychol 116:158–163

Mason MJ, Cornwall HL, Smith ESJ (2016) Ear structures of the naked mole-rat, *Heterocephalus glaber*, and its relatives (Rodentia: Bathyergidae). PLoS ONE 11:e0167079

McClure TD, Daron GH (1971) The relationship of the developing inner ear, subarcuate fossa and paraflocculus in the rat. Am J Anat 130:235–249

McLaren JW, Hillman DE (1979) Displacement of the semicircular canal cupula during sinusoidal rotation. Neuroscience 4:2001–2008

McVean A (1999) Are the semicircular canals of the European mole, *Talpa europaea*, adapted to a subterranean habitat? Comp Biochem Physiol Part A Mol Integr Physiol 123:173–178

Mittelstaedt H (1999) The role of the otoliths in perception of the vertical and in path integration. Ann N Y Acad Sci 871:334–344

Muller M (1999) Size limitations in semicircular duct systems. J Theor Biol 198:405–437

Muller M, Verhagen JHG (2002) Optimization of the mechanical performance of a two-duct semicircular duct system—part 2: excitation of endolymph movements. J Theor Biol 216:425–442

Narins PM, Lewis ER, Jarvis JJ, O'Riain J (1997) The use of seismic signals by fossorial southern African mammals: a neuroethological gold mine. Brain Res Bull 44:641–646

Obrist D (2011) Fluid mechanics of the inner ear. Habilitation treatise in fluid mechanics at the department of mechanical and process engineering of ETH Zurich. Zurich

Oman CM, Marcus EN, Curthoys IS (1987) The influence of semicircular canal morphology on endolymph flow dynamics. An anatomically descriptive mathematical model. Acta Otolaryngol 103:1–13

Pfaff C, Martin T, Ruf I (2015) Bony labyrinth morphometry indicates locomotor adaptations in the squirrel-related clade (Rodentia, Mammalia). Proc R Soc B 282:20150744

Pfaff C, Czerny S, Nagel D, Kriwet J (2017) Functional morphological adaptations of the bony labyrinth in marsupials (Mammalia, Theria). J Morphol 278:742–749

Rabbitt RD, Damiano ER, Grant WJ (2004) Biomechanics of the semicircular canals and otolith organs. In: Highstein SM, Fay RR (eds) The vestibular system. Springer, New York, pp 153–201

Rabbitt RD, Breneman KD, King C et al (2009) Dynamic displacement of normal and detached semicircular canal cupula. J Assoc Res Otolaryngol 10:497–509

Rambold H, Churchland A, Selig Y et al (2002) Partial ablations of the flocculus and ventral paraflocculus in monkeys cause linked deficits in smooth pursuit eye movements and adaptive modification of the VOR. J Neurophysiol 87:912–924

Revell LJ (2012) phytools: an R package for phylogenetic comparative biology (and other things). Methods Ecol Evol 3:217–223

Rodgers JC (2011) Comparative morphology of the vestibular semicircular canals in therian mammals. Dissertation, University of Texas

Shaikh A, Wang F (2021) Eye movements and vestibular dysfunction: lesions of cerebellum. Eye Movements in the Critical Care Setting. Springer, Cham

Silcox MT, Bloch JI, Boyer DM et al (2009) Semicircular canal system in early primates. J Hum Evol 56:315–327

Spoor F, Zonneveld F (1998) Comparative review of the human bony labyrinth. Am J Phys Anthropol 107:211–251

Spoor F, Wood B, Zonneveld F (1994) Implications of early hominid labyrinthine morphology for evolution of human bipedal locomotion. Nature 369:645–648

Spoor F, Garland T, Krovitz G et al (2007) The primate semicircular canal system and locomotion. Proc Natl Acad Sci U S A 104:10808–10812

Stackman RW, Herbert AM (2002) Rats with lesions of the vestibular system require a visual landmark for spatial navigation. Behav Brain Res 128:27–40

Steer RW, Li, Yao T, Young LR, Meiry JL (1967) Physical properties of the labyrinthine fluids and quantification of the phenomenon of caloric stimulation. In: Ashton Graybiel (ed) Third symposium on the role of the vestibular organs in space exploration. NASA, Pensacola, pp 409–420

Tambusso PS, Varela L, Góis F et al (2021) The inner ear anatomy of glyptodonts and pampatheres (Xenarthra, Cingulata): functional and phylogenetic implications. J South Am Earth Sci 108:103189

Upham NS, Esselstyn JA, Jetz W (2019) Inferring the mammal tree: species-level sets of phylogenies for questions in ecology, evolution, and conservation. PLoS Biol 17:1–44

Urciuoli A, Zanolli C, Almécija S et al (2021) Reassessment of the phylogenetic relationships of the late Miocene apes *Hispanopithecus* and *Rudapithecus* based on vestibular morphology. Proc Natl Acad Sci U S A 118:e2015215118

Vleck D (1979) The energy cost of burrowing by the pocket gopher *Thomomys bottae*. Physiol Zool 52:122–136

Wilkie HC (1925) The auditory apparatus of the common mole, *Talpa europaea*. Proc Zool Soc Lond 95:1281–1292

Xiong G, Nagao S (2002) The lobulus petrosus of the paraflocculus relays cortical visual inputs to the posterior interposed and lateral cerebellar nuclei: an anterograde and retrograde tracing study in the monkey. Exp Brain Res 147:252–263

Xiong G, Nagao S, Kitazawa H (2010) Mossy and climbing fiber collateral inputs in monkey cerebellar paraflocculus lobulus petrosus and hemispheric lobule VII and their relevance to oculomotor functions. Neurosci Lett 468:282–286

Yoder RM, Taube JS (2014) The vestibular contribution to the head direction signal and navigation. Front Integr Neurosci 8:32

Zee DS, Yamazaki A, Butler PH, Gücer E (1981) Effects of ablation of flocculus and paraflocculus on eye movements in primate. J Neurophysiol 46:878–899